

MAGNETIC RELAXATION, CURRENT SHEETS, AND STRUCTURE FORMATION IN AN EXTREMELY TENUOUS FLUID MEDIUM

K. BAJER¹ AND H. K. MOFFATT²

¹ Institute of Geophysics, Warsaw University, ul. Pasteura 7, 02-093 Warszawa, Poland

² Department of Applied Mathematics and Theoretical Physics, University of Cambridge, Wilberforce Road, Cambridge CB3 0WA, UK
Received 2013 June 4; accepted 2013 October 3; published 2013 December 3

ABSTRACT

The process of relaxation of a unidirectional magnetic field in a highly conducting tenuous fluid medium is considered. Null points of the field play a critical role in this process. During an initial stage of relaxation, variations in magnetic pressure are eliminated, and current sheets build up in the immediate neighborhood of null points. This initial phase is followed by a long diffusive phase of slow algebraic decay of the field, during which fluid is continuously sucked into the current sheets, leading to exponential growth of fluid density and concentration of mass around the null points, which show a tendency to cluster. Ultimately, this second phase of algebraic decay gives way to a final period of exponential decay of the field. The peaks of density at the null points survive as a fossil relic of the decay process. Numerical solution of the governing equations provides convincing confirmation of this three-stage scenario. Generalizations to two- and three-dimensional fields are briefly considered.

Key words: intergalactic medium – ISM: kinematics and dynamics – ISM: structure – large-scale structure of universe – magnetic fields – magnetic reconnection

Online-only material: color figures

1. INTRODUCTION

When a conducting fluid, initially at rest, is permeated by a non-uniform magnetic field, the associated Lorentz force in general drives motion in the fluid. Magnetic energy is converted to kinetic energy, which is dissipated by viscosity, and also in part to internal energy if the fluid is compressible. If the fluid is regarded as perfectly conducting, then the field lines are frozen in the fluid, and the topology of the field is conserved. There is thus a tendency for the magnetic field to relax in such a way that the sum of magnetic and internal energies decreases to a minimum subject to the constraints of the conserved topology of the field and any boundary conditions that may be applicable.

This process, originally conceived by Arnold (1974), has been analyzed in some detail for both incompressible and compressible barotropic fluids (Moffatt 1985, 1987). In both cases, it was shown that tangential discontinuities of the magnetic field (i.e., current sheets) are an almost inevitable outcome of this relaxation process. The inevitability of current sheets in the magnetostatic equilibria of any nontrivial topological field structure is the subject of Parker’s (1994) book *Spontaneous Current Sheets in Magnetic Fields*, in which the relevance of the phenomenon in the context of solar flares and coronal heating is thoroughly discussed.

Despite the importance of this field of application in solar physics, and equally in the extremely tenuous interstellar and intergalactic media, the details of the actual process of relaxation and of the effects of finite magnetic resistivity have remained elusive (except in the case of two-dimensional (2D) fields in incompressible fluid, as studied by Linardatos 1993). There are two principal difficulties: (1) conservation of field topology is difficult to incorporate adequately in three-dimensional (3D) numerical simulations; and (2) although the trend toward the formation of current sheets may be detected numerically, it is virtually impossible to continue numerical simulations all the way to the singular limit (when resistivity is set to zero).

In this paper, we consider an idealized one-dimensional model for which these difficulties can be overcome and the relaxation process can be fully understood. The magnetic field is assumed unidirectional and the medium extremely tenuous so that the dynamic effects of fluid pressure can be neglected. For simplicity, we also neglect fluid inertia³ (justifiable when the density is sufficiently small), but we retain viscosity as the energy-dissipating mechanism. In this situation, the internal energy and the kinetic energy of the fluid are negligible compared with the magnetic energy, and it is therefore just this magnetic energy that seeks a minimum. The minimum-energy state is “force-free” and does indeed involve current sheets, which form in the immediate neighborhood of null points of the field. When weak resistivity effects are taken into account, the structure of these sheets may be determined, and the resulting relatively slow decay of the global magnetic field may then be deduced. This is essentially a “matched asymptotic” calculation, in which an understanding of the formation and structure of the current sheets is a necessary preliminary to calculating the overall long-term evolution of the field.

The persistent erosion of the magnetic field at null points implies that the magnetic pressure remains permanently minimal there. Fluid is therefore continuously “sucked in” toward these points by the deficit of magnetic pressure. The resulting buildup of density in the neighborhood of null points can be quite dramatic, as will be shown in Section 6—see particularly Figure 10, which shows how the peak density can increase by a factor of 10^5 or more, depending on the magnitude of the dimensionless number S (defined in Equation (13) below), the sole parameter relevant to what emerges as a three-stage relaxation process.

As background to this investigation, we may cite the wide-ranging review by Kulsrud & Zweibel (2008) of theories of the origin and dynamo evolution of the magnetic field in the ultra-low-density protogalactic medium; see also Grasso & Rubinstein (2001), who present arguments in favor of a

³ Fluid inertia can be included without changing the essential relaxation mechanism.

primordial origin of magnetic fields in the cosmos, and Banerjee & Jedamzik (2004), who discuss the evolution of cosmic magnetic fields from the very early universe to the present era. In more recent work, Pfrommer & Dursi (2010) and Doumler & Knebe (2010) discuss the influence of magnetic fields upon structure formation in the universe. The possibility that primordial magnetic fields can trigger early structure formation is suggested by the investigations of Sethi & Subramanian (2005) and Tashiro & Sugiyama (2006). These works lend motivation to the present study, which exhibits in fine detail how structure can emerge from a simple magnetohydrodynamic (MHD) relaxation and diffusion process.

Some of the broader considerations concerning topological jumps have been recently reviewed by Goldstein et al. (2012), and the manner in which such jumps can be realized in soap-film experiments (in which energy, proportional to soap-film area, is minimized) has been demonstrated by Goldstein et al. (2010).

2. ONE-DIMENSIONAL RELAXATION IN A PRESSURELESS FLUID

The relaxation of a magnetic field in a viscous compressible fluid is described by the MHD equations, i.e., in standard notation:

$$\rho \frac{D\mathbf{u}}{Dt} = -\nabla p + \mathbf{j} \wedge \mathbf{B} + \mu_s \nabla^2 \mathbf{u} + \left(\frac{1}{3}\mu_s + \mu_b\right) \nabla(\nabla \cdot \mathbf{u}), \quad (1a)$$

$$\frac{\partial \rho}{\partial t} + \nabla \cdot (\rho \mathbf{u}) = 0, \quad (1b)$$

$$\frac{\partial \mathbf{B}}{\partial t} = \nabla \wedge (\mathbf{u} \wedge \mathbf{B}) + \eta \nabla^2 \mathbf{B}, \quad \nabla \cdot \mathbf{B} = 0. \quad (1c)$$

Here the current \mathbf{j} is given by⁴ $\mathbf{j} = \nabla \times \mathbf{B}$, and μ_s , μ_b , and η are, respectively, the coefficients of shear and bulk viscosity and the magnetic diffusivity of the fluid. In general, these equations must be supplemented by an equation of state relating pressure p and density ρ ; however, we shall be concerned here with an extremely tenuous fluid (i.e., an extremely low- β plasma) in which the pressure gradient ∇p can in effect be set to zero. Further, for greater simplicity, we shall suppose that the density is so low that the inertia term $\rho D\mathbf{u}/Dt$ in Equation (1a) is also negligible. In this situation, from Equation (1a), the velocity \mathbf{u} is instantaneously related to the magnetic field \mathbf{B} by the quasi-static (or “diagnostic”) equation:

$$\mu_s \nabla^2 \mathbf{u} + \left(\frac{1}{3}\mu_s + \mu_b\right) \nabla(\nabla \cdot \mathbf{u}) = -\mathbf{j} \wedge \mathbf{B}, \quad (2)$$

while \mathbf{B} evolves according to Equation (1c); the density ρ plays a subsidiary role, evolving as a passive scalar field. Magnetoacoustic oscillations and waves are filtered from the equations in this approximation.

We consider the simplest possible configuration: a unidirectional magnetic field of the form

$$\mathbf{B} = B(x, t) \hat{\mathbf{e}}_z, \quad (3)$$

with initial condition $B(x, 0) = B_{in}(x)$. Then

$$\mathbf{j} = -\frac{\partial B}{\partial x} \hat{\mathbf{e}}_y \quad \text{and} \quad \mathbf{j} \times \mathbf{B} = -\frac{\partial}{\partial x} \left(\frac{1}{2} B^2\right) \hat{\mathbf{e}}_x. \quad (4)$$

We shall suppose that $\partial B_{in}(x)/\partial x$ is everywhere finite.

The (driven) velocity field then also has the one-dimensional form $\mathbf{u} = u(x, t) \hat{\mathbf{e}}_x$, where, from Equation (2),

$$\mu \frac{\partial^2 u}{\partial x^2} = \frac{\partial}{\partial x} \left(\frac{1}{2} B^2\right), \quad (5)$$

with $\mu = (4/3)\mu_s + \mu_b$ (the “effective viscosity” in this one-dimensional situation). This integrates immediately to give

$$\mu \frac{\partial u}{\partial x} = \frac{1}{2} B^2 + F(t), \quad (6)$$

for some function $F(t)$. We shall suppose that B and u are either periodic or stationary-random functions of x , with zero mean; then evidently $F(t) = -(1/2)\langle B^2 \rangle$, and

$$\mu \frac{\partial u}{\partial x} = \frac{1}{2} (B^2 - \langle B^2 \rangle), \quad (7)$$

where the angular brackets denote an average over x . At the same time, the induction Equation (1c) reduces to

$$\frac{\partial B}{\partial t} = -\frac{\partial}{\partial x} (uB) + \eta \frac{\partial^2 B}{\partial x^2}. \quad (8)$$

An energy equation may be obtained by standard manipulation of Equations (5) and (8) in the form

$$\begin{aligned} \frac{\partial}{\partial t} \frac{1}{2} B^2 &= \frac{\partial}{\partial x} \left(-uB^2 + \mu u \frac{\partial u}{\partial x} + \eta B \frac{\partial B}{\partial x} \right) \\ &\quad - \mu \left(\frac{\partial u}{\partial x} \right)^2 - \eta \left(\frac{\partial B}{\partial x} \right)^2. \end{aligned} \quad (9)$$

For periodic or stationary-random conditions, the x -average of the first term on the right is zero, so averaging over x and using Equation (7), we obtain

$$\frac{d}{dt} \langle B^2 \rangle = -\frac{1}{2\mu} \langle (B^2 - \langle B^2 \rangle)^2 \rangle - 2\eta \langle (\partial B / \partial x)^2 \rangle. \quad (10)$$

The first term on the right indicates a tendency for B^2 to evolve toward its average value $\langle B^2 \rangle$ everywhere, i.e., for B to evolve to $\pm \sqrt{\langle B^2 \rangle}$ accordingly as $B >$ or $<$.

Points where $B(x, t) = 0$ (null points⁵ of the field) play a prominent role in the relaxation process. In general, $\partial B / \partial x$ is non-zero at null points, so that B changes sign at each such point. We shall suppose, unless otherwise stated, that all null points are “generic” in this sense.

We may distinguish two stages in this process. The first stage is non-diffusive, and the flux between any two null points is conserved. It follows that the mean “unsigned” flux $\langle |B(x, t)| \rangle$ is also conserved; it is therefore useful to define

$$B_0 \stackrel{\text{def}}{=} \langle |B(x, 0)| \rangle, \quad (11)$$

and to use this as the scale of the magnetic field, conserved during the initial phase. The field relaxation during this phase proceeds on the timescale

$$t_r \stackrel{\text{def}}{=} \mu / B_0^2 = \delta_m^2 / \eta, \quad \text{where} \quad \delta_m^2 = \mu \eta / B_0^2. \quad (12)$$

⁵ The points $x = x_n$ are strictly “null planes” in the space of the Cartesian coordinates (x, y, z) , but we shall refer to them as null points throughout, without danger of misunderstanding.

⁴ The permeability of the vacuum, μ_0 , is absorbed in the definition of \mathbf{B} .

During this phase, current sheets tend to form in the neighborhood of null points of B . The thickness of these sheets decreases to a minimum scale, of order δ_m , at which the two terms on the right of Equation (8) become comparable in magnitude. This first stage is followed by a much slower second stage when weak diffusion slowly erodes the current sheets through a non-linear but quasi-static process.

This scenario requires that the scale of the initial field, L say, be large compared with δ_m , i.e., that⁶

$$S \stackrel{\text{def}}{=} \frac{L}{\delta_m} = \frac{B_0 L}{\sqrt{\mu \eta}} \gg 1. \quad (13)$$

We assume that this condition is satisfied in the discussion that follows. For fields that are periodic in x , we shall take L to be the half-period. Alternatively, it may be more appropriate to use the typical separation of null points, \bar{L} say, with corresponding $\bar{S} = \bar{L}/\delta_m$.

We shall find in Section 4 that the second (diffusive) stage lasts for a period $t_d = O(S^2)t_r$; during this stage, the field decays algebraically and the timescale of decay $|d(\ln B)/dt|^{-1}$ increases from $O(S)t_r$ to $O(S^2)t_r$. For $t > S^2 t_r$, the field is so weak that the first term on the right of Equation (8) becomes negligible, and a ‘‘final period of decay’’ sets in with exponential decay on the timescale t_d .

We shall show in Section 6 that the density field tends to concentrate at the null points; this concentration persists during the long diffusive stage when the density at the null points increases to a saturation level ρ_s that increases exponentially with S . For example, even for the modest value $S = 50$, ρ_s/ρ_0 is already greater than 2×10^5 , where ρ_0 is the initial density, assumed uniform. The set of density concentrations survives as a ‘‘fossil relic’’ of the relaxation process after the ultimate decay of the magnetic field.

3. INITIAL STAGE: NON-DIFFUSIVE RELAXATION

In this section, we set $\eta = 0$ (equivalently $S = \infty$), i.e., we neglect effects of magnetic diffusion. In this perfectly conducting limit, the \mathbf{B} -lines are frozen in the fluid, with conservation of magnetic flux across any Lagrangian (material) surface. Equations (1b) and (8) then together imply that

$$\frac{D}{Dt} \left(\frac{B}{\rho} \right) = \left(\frac{\partial}{\partial t} + u \frac{\partial}{\partial x} \right) \left(\frac{B}{\rho} \right) = 0, \quad (14)$$

so that B/ρ is constant following any material particle. In particular, the null points of $B(x, t)$ move with the fluid. Suppose that these null points are located at $x = x_n(t)$ ($n = 0, \pm 1, \pm 2, \pm 3, \dots$). Let $I_n(t)$ denote the open interval (x_n, x_{n+1}) of length $\Delta_n(t) = x_{n+1} - x_n$. In each I_n , B is nonzero (positive or negative), and the flux in each interval,

$$\Phi_n = \int_{I_n} B(x, t) dx, \quad (15)$$

is conserved during the relaxation process.

3.1. Energy Minimization

The null points and the corresponding intervals move during relaxation and eventually settle in their final positions:

$$x_n(t) \rightarrow x_n^f, \quad I_n(t) \rightarrow I_n^f, \quad \text{and} \quad \Delta_n(t) \rightarrow \Delta_n^f \quad \text{as} \quad t \rightarrow \infty. \quad (16)$$

Let B_n denote the average of the relaxed field in the interval I_n^f , i.e.,

$$B_n = \frac{1}{\Delta_n^f} \int_{I_n^f} B(x) dx = \frac{\Phi_n}{\Delta_n^f}. \quad (17)$$

Then the energy in the interval I_n^f is

$$E_n = \frac{1}{2} \int_{I_n^f} B^2(x) dx \equiv \frac{1}{2} \int_{I_n^f} ((B(x) - B_n)^2 + B_n^2) dx. \quad (18)$$

The minimizing field in I_n^f is therefore $B(x) = B_n$ and thus constant. Hence, in the relaxed state the field is piecewise constant on open intervals between the null points. At a generic null point the field changes sign and therefore exhibits a tangential discontinuity, i.e., a current sheet.

In fact, the condition for *global equilibrium* requires the *magnitude* of the field, $|B_n|$, to have the same value in *all* intervals $n = 1 \dots N-1$. This can be demonstrated in two ways. First, if $|B_n| \neq |B_{n+1}|$, then there would be an unsustainable pressure jump across the null located at x_n^f . Second, the state with all B_n equal minimizes the *total* magnetic energy $\langle E \rangle$.

We calculate the variation of $\langle E \rangle = \sum_{n=1}^{N-1} E_n$ ($N \geq 2$), where $E_n = (1/2)(\Phi_n/\Delta_n)^2 \Delta_n$ is the energy in the interval Δ_n . The fluxes Φ_n are prescribed, while the positions of the nulls (and therefore the lengths Δ_n of the intervals) are variable, except for the end points at $x = 0$ and $x = L$, which are fixed and thus impose the constraint $\sum_{n=1}^{N-1} \Delta_n = L$. The (constrained) minimization of the total energy then gives

$$\begin{aligned} \delta \left[\sum_{n=1}^{N-1} \frac{1}{2} \left(\frac{\Phi_n}{\Delta_n} \right)^2 \Delta_n + \lambda \sum_{n=1}^{N-1} \Delta_n \right] \\ = - \sum_{n=1}^{N-1} \left[\frac{1}{2} \left(\frac{\Phi_n}{\Delta_n} \right)^2 - \lambda \right] \delta \Delta_n = 0, \end{aligned} \quad (19)$$

where λ is a Lagrange multiplier. Hence, indeed the magnitude of the field is the same in all subintervals, and only its sign changes at the null points:

$$B_n = \frac{\Phi_n}{|\Phi_n|} B_0, \quad \text{where now} \quad B_0 = \frac{1}{L} \int_0^L |B_0(x)| dx. \quad (20)$$

The final positions of the interior null points are then also determined; these are at positions

$$x_n^f = \sum_{m=1}^{n-1} \Delta_m^f \quad (n = 2, 3, \dots, N-1), \quad \text{where} \quad \Delta_m^f = |\Phi_m|/B_0. \quad (21)$$

Similarly, since the flux between *any* two material points is conserved, knowledge of the final state allows us to infer the net displacement of *every* material point over the entire relaxation process, and hence the corresponding net change in the density distribution (see Section 6 below for an explicit calculation).

In summary, relaxation in a perfectly conducting pressureless fluid eliminates variations in magnetic pressure, smooths all

⁶ Note that $S = Lu/\sqrt{\text{Pr}_m}$, where $Lu = V_A L/\nu$ is the Lundquist number and $\text{Pr}_m = \nu/\lambda$ the magnetic Prandtl number (with $\nu = \mu/\rho_0$ and $V_A = B_0/\sqrt{\rho_0}$ the Alfvén velocity based on the initial density ρ_0 , assumed uniform).

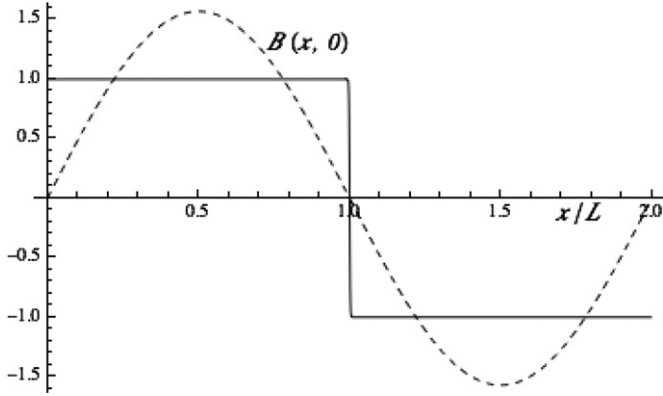


Figure 1. Relaxation of the field $B(x, 0) = (\pi/2)\sin(\pi x/L)$ (dashed), to a piecewise constant field with tangential discontinuity at $x = L$ (solid).

field variations between null points, and creates current sheets and density concentrations at these null points. The situation is illustrated in Figure 1 for the prototype initial field $B(x, 0) = (\pi/2)\sin(\pi x/L)$ ($0 < x/L < 2$), for which $B_0 = 1$.

3.2. Exponential Development of Current Sheets

The time-dependent approach to the current sheet limit in the above non-diffusive situation is of interest. We focus on an isolated current sheet of the above type, near a null point of B located at, say, $x = 0$, and we suppose that B tends to the values $\pm B_0$ outside the sheet. Let L be the typical distance between null points of B . Adopting dimensionless variables

$$x^* = x/L, \quad t^* = t/t_r, \quad B^* = B/B_0, \quad \text{and} \quad u^* = u(t_r/L), \quad (22)$$

and dropping the stars, Equations (8) and (7) become

$$\frac{\partial B}{\partial t} = -\frac{\partial(uB)}{\partial x} + \frac{1}{S^2} \frac{\partial^2 B}{\partial x^2}, \quad \frac{\partial u}{\partial x} = \frac{1}{2}(B^2 - 1), \quad (23)$$

with the (now scaled) boundary conditions

$$B(x, t) \sim \pm 1 \quad \text{as} \quad x \rightarrow \pm\infty. \quad (24)$$

With $S \gg 1$, Equations (23) become, in first approximation,

$$\frac{\partial B}{\partial t} = -\frac{\partial(uB)}{\partial x}, \quad \frac{\partial u}{\partial x} = \frac{1}{2}(B^2 - 1). \quad (25)$$

These equations describe the “non-diffusive” first phase of development of the current sheet, once the “plateaus” with $B = \pm 1$ have formed on either side of the sheet. We may assume that the fields B and u are antisymmetric,

$$B(-x, t) = -B(x, t), \quad u(-x, t) = -u(x, t), \quad (26)$$

and we look for a similarity solution of the form

$$B(x, t) = f(\xi), \quad \text{where} \quad \xi = x/\delta(t). \quad (27)$$

Then, from Equation (25),

$$u(x, t) = \frac{1}{2}\delta(t)v(\xi), \quad \text{where} \quad v'(\xi) = f(\xi)^2 - 1, \quad (28)$$

and it follows that

$$(\delta/\delta)\xi f'(\xi) = \frac{1}{2}(vf)'. \quad (29)$$

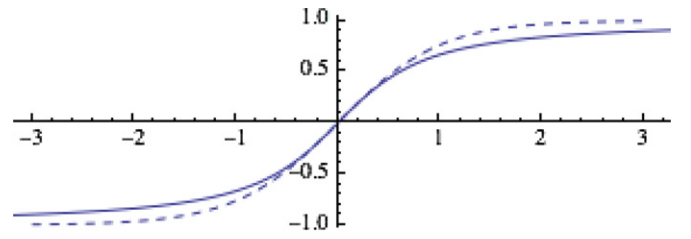


Figure 2. Function $f(\xi)$ (solid) given by Equation (35), with $C = 1$, $D = 0$. The function $\tanh \xi$ (dashed) is shown for comparison.

(A color version of this figure is available in the online journal.)

We can satisfy this only if

$$\delta/\delta = -k \quad (\text{const.}), \quad \text{i.e.,} \quad \delta(t) \sim e^{-kt}. \quad (30)$$

Equations (25) now reduce to

$$(vf)' = -2k\xi f' \quad \text{and} \quad v' = f^2 - 1. \quad (31)$$

Eliminating $v(\xi)$ and simplifying, we get

$$f(f^2 - 1)f'' = 2(2f^2 + k - 1)f'^2, \quad (32)$$

and the appropriate boundary conditions (consistent with the antisymmetry condition $f(-\xi) = -f(\xi)$) are

$$f(0) = 0, \quad f(\infty) = 1. \quad (33)$$

The first of these is compatible with Equation (32) only if $k = 1$; then Equation (32) integrates once to give

$$f' = C(f^2 - 1)^2, \quad (34)$$

where C is a constant; by rescaling ξ (equivalent to the freedom of choice of time origin in Equation (30)), we may take $C = 1$. A second integration with the boundary condition $f(0) = 0$ then gives

$$\frac{1}{4} \left[\frac{2f}{1-f^2} + \ln \frac{1+f}{1-f} \right] = \xi. \quad (35)$$

The function $f(\xi)$, obtained by inverting this equation, is plotted in Figure 2, with the function $\tanh \xi$ (dashed) shown for comparison. The asymptotic behavior of $f(\xi)$ is

$$f \sim \xi \quad \text{for} \quad \xi \rightarrow 0, \quad \text{and} \quad f \sim 1 - \frac{2}{\xi} \quad \text{as} \quad \xi \rightarrow \infty. \quad (36)$$

Now $v(\xi)$ can be found from Equation (31); the only problem is that this behaves logarithmically for large ξ :

$$v(\xi) \sim -4 \ln \xi \rightarrow -\infty \quad \text{as} \quad \xi \rightarrow \infty. \quad (37)$$

However, realistically ξ is never greater than $O(S)$; moreover, from Equation (28),

$$u(x, t) \sim \frac{1}{2}v(\xi)e^{-t}, \quad (38)$$

so that exponential decay wins in the end!

For the prototype initial field shown in Figure 1, the magnetic energy $(1/2)\langle B^2 \rangle$ decreases during the initial stage from $\pi^2/16 \approx 0.61685$ to 0.5. This decrease, at least once the plateaus have formed, is well represented by the function

$$\langle B^2 \rangle(t) = \frac{\pi^2}{\pi^2 + (8 - \pi^2)e^{-t}}, \quad (39)$$

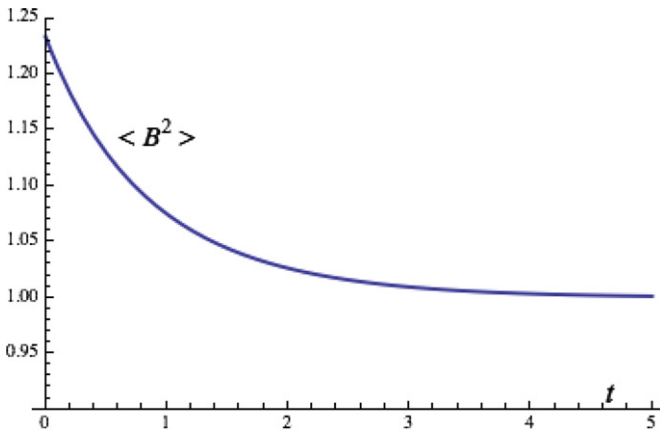


Figure 3. Schematic representation of the non-diffusive relaxation of magnetic energy; when $t = O(\ln S)$, diffusion becomes significant.

(A color version of this figure is available in the online journal.)

as shown in Figure 3. Note that the length scale $\delta(t)$ decreases exponentially during this non-diffusive stage. If the initial scale is $O(L)$, this continues only until

$$L e^{-t} = O(\delta_m) \quad \text{or equivalently until} \quad t = O(\ln S). \quad (40)$$

At this stage, as may be easily verified, the diffusive term $S^{-2} \partial^2 B / \partial x^2$ becomes of the same order of magnitude as $\partial B / \partial t$. In dimensional terms, the non-diffusive phase lasts for the period $0 < t < O(\ln S)t_r$. The current sheet develops exponentially rapidly during this phase, the scale decreasing exponentially in time until it reaches the scale δ_m , when diffusion can no longer be neglected.

4. SLOW DIFFUSION PHASE

4.1. Steady State of a Dissipating Current Sheet

We turn now to the second “diffusive” stage of evolution. Consider first the possibility of an isolated *steady* current sheet with thickness $O(\delta_m)$, located in the neighborhood of $x = 0$. The length L is now irrelevant, and the appropriate dimensionless variables are

$$x^{**} = x/\delta_m, \quad u^{**} = (\delta_m/\eta)u, \quad \text{and still} \quad B^* = B/B_0. \quad (41)$$

Substituting in Equations (8) and (7), and again dropping the stars, the steady equations become

$$B'' = (uB)', \quad u' = \frac{1}{2}(B^2 - 1), \quad (42)$$

with boundary conditions

$$B \rightarrow \pm 1 \quad \text{and} \quad u \rightarrow \mp u_0 \quad \text{as} \quad x \rightarrow \pm \infty. \quad (43)$$

Integrating the first of Equations (42) with these boundary conditions gives

$$B' = uB + u_0, \quad u' = \frac{1}{2}(B^2 - 1). \quad (44)$$

The energy Equation (9) integrates to give

$$\int_{-\infty}^{\infty} (u^2 + B^2) dx = [-uB^2 + uu' + BB']_{-\infty}^{\infty} = 2u_0, \quad (45)$$

which shows immediately that a nontrivial steady state is possible only if $u_0 > 0$. This means that, as might be expected, the fluid must flow into the current sheet from both sides. This is not therefore a strictly steady-state situation, because the fluid density must increase continuously in time within the sheet; however, for as long as the pressure remains negligible, the fields B and u can still remain steady. The implications for the buildup of density in the sheet will be considered in Section 6.

Equations (44) together with the boundary conditions (43) constitute a nonlinear eigenvalue problem. Figure 4 shows the phase portrait for three values of u_0 . As u_0 increases from zero to $1 + 1/\sqrt{2}$, the phase portrait evolves continuously, and for the critical value $u_0 = 1/\sqrt{2}$ it exhibits a heteroclinic connection between the fixed points $(-1, u_0)$ and $(1, -u_0)$ in the (B, u) -plane (corresponding to $x = \mp \infty$, respectively). In Figure 4(b), it is evident that this heteroclinic connection is a straight line, which suggests looking for a solution in the form $B = -u/u_0$ (consistent with the conditions at $x = \pm \infty$). With $u_0 = 1/\sqrt{2}$ this solution is easily found in the form

$$B = -\sqrt{2} u = \tanh(x/\sqrt{2}). \quad (46)$$

This describes a dissipating current sheet in a pressureless fluid of effectively infinite extent. Positive magnetic field in the half-space $x > 0$ and negative field in the half-space $x < 0$ are pressed together by a converging flow driven by the magnetic pressure gradient, moderated by viscosity. Magnetic diffusion in the current sheet annihilates the field and thus maintains the magnetic pressure gradient that drives the flow. The thickness and structure of the sheet and the inflow are uniquely determined by the conditions $B(x) \rightarrow \pm 1$ as $x \rightarrow \pm \infty$ and the resulting internal balance. (This is in marked contrast to a “conventional” current sheet in an incompressible fluid where the inflow can be specified independently and the sheet adjusts its thickness accordingly.) Returning to dimensional variables, the sheet thickness is indeed $O(\delta_m)$ and, from Equations (41) and (46), the inflow velocity is precisely

$$u_0 = \eta/(\sqrt{2} \delta_m) = \sqrt{\eta/2\mu} B_0. \quad (47)$$

4.2. Similarity Solution during Diffusive Phase

The above steady solution applies only to a single isolated current sheet. But now consider any two null points of $B(x, t)$, which, without loss of generality, we may take to be centered on $x = 0$ and $x = L$, with $L \gg \delta_m$ (i.e., $x = S$ when x is scaled with δ_m). We suppose for the moment that these null points are fixed, and that the field is uniform, $\bar{B}(t)$ say, except in the current sheets near the null points, so that the flux between them is approximately $\bar{B}(t)L$; we assume this to be positive. The result (47) corresponds to the situation when in effect $L = \infty$; now, with $S = L/\delta_m$ sufficiently large, we may anticipate quasi-steady evolution with Equation (47) still satisfied. Integrating Equation (8) between δ_m and $L - \delta_m$, (i.e., over the plateau region in which B is uniform), the slow decrease of flux $\bar{B}(t)L$ is given approximately by

$$\frac{d}{dt}(\bar{B}(t)L) = -2|u_0|\bar{B} = -\sqrt{\frac{2\eta}{\mu}} \bar{B}^2, \quad (48)$$

using Equation (47). With the scaling (41), together with $t^* = t/t_r$ and $\bar{B}^* = \bar{B}/B_0$, this equation becomes in dimensionless

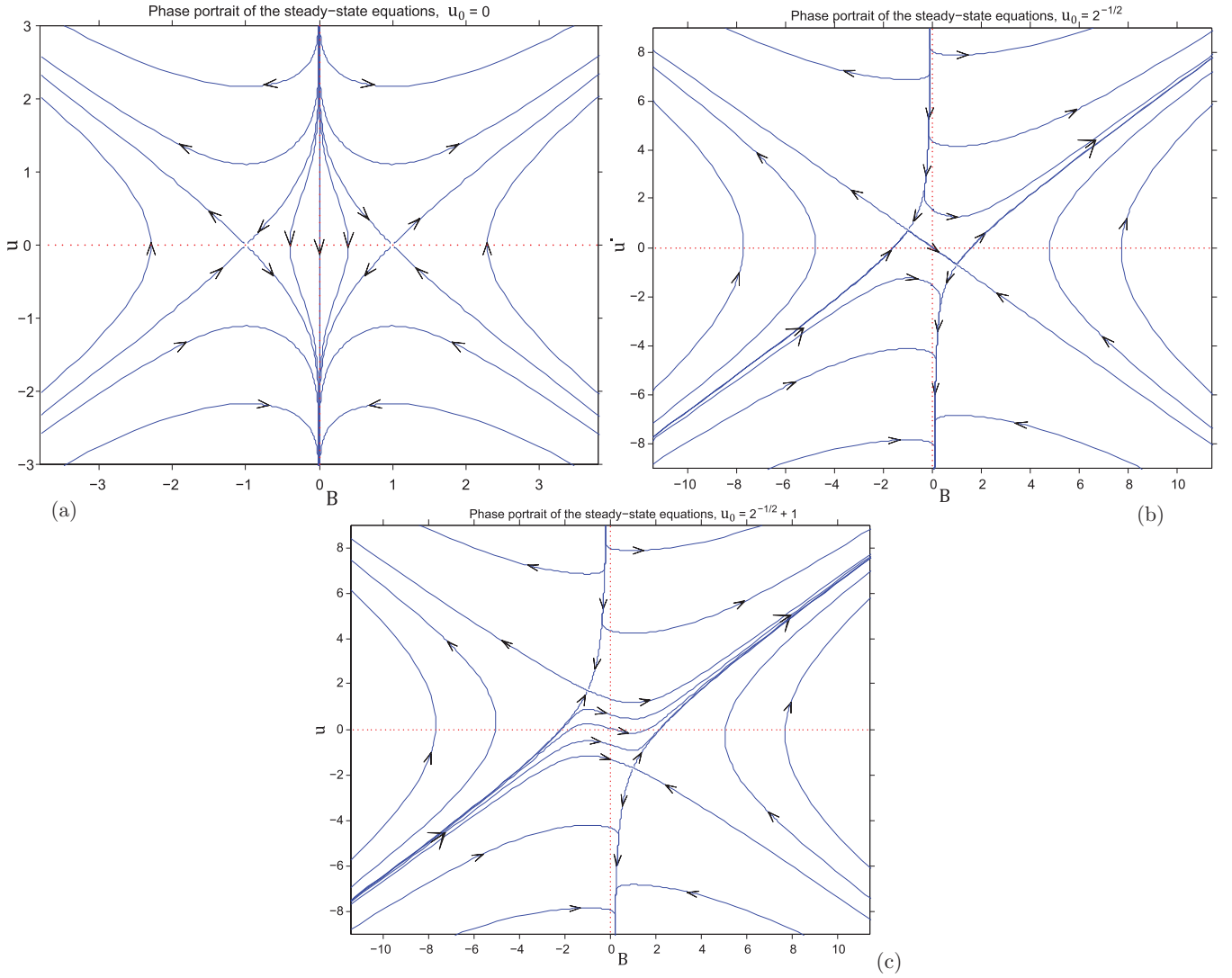


Figure 4. Phase portrait of Equations (44) for (a) $u_0 = 0$, (b) $u_0 = 1/\sqrt{2}$, and (c) $u_0 = 1/\sqrt{2} + 1$. Arrows show the direction of increasing x . (A color version of this figure is available in the online journal.)

form

$$\frac{d}{dt} \frac{1}{\bar{B}} = \frac{\sqrt{2}}{S}, \quad (49)$$

which integrates to give

$$\bar{B}(t) = \frac{S}{\sqrt{2}(t + t_1)}, \quad (50)$$

where t_1 is a constant of integration. Since $\bar{B} = O(1)$ when $t = 0$, it follows that $t_1 = O(S)$. The situation is represented schematically in Figure 5, with current sheets at $x/S = 0$ and ± 1 .

During this diffusive phase, each current sheet evolves slowly as a result of this decay. Again with the scaling (41), the anticipated quasi-static evolution is described by

$$\frac{\partial^2 B}{\partial x^2} = \frac{\partial}{\partial x}(uB), \quad (51a)$$

$$\frac{\partial u}{\partial x} = \frac{1}{2}(B^2 - \langle B^2 \rangle). \quad (51b)$$

For the sheet at $x = 0$, the boundary conditions are

$$B(0, t) = 0, \quad B(x, t) \sim \bar{B}(t) = \frac{S}{\sqrt{2}(t + t_1)} \quad \text{as } x \rightarrow \infty. \quad (52)$$

Here, t appears merely as a parameter.⁷

Note that the velocity field $u(x, t)$ in each plateau region has uniform gradient $\partial u/\partial x = 1/(t + t_1)$, satisfying Equation (8). Since u is antisymmetric about $x = S/2$, it follows that, in the plateau region between $x = 0$ and $x = S$,

$$u(x, t) = \frac{(x - S/2)}{t + t_1}. \quad (53)$$

This implies that, at the outer limits of the current sheets at $x = 0$ and $x = S$,

$$u = \mp \frac{S}{2(t + t_1)} = \mp \frac{\bar{B}}{\sqrt{2}}, \quad (54)$$

⁷ Strictly this requires antisymmetry about $x = 0$. If current sheets are distributed non-uniformly in x , then they will move during decay in such a way as to maintain magnetic pressure equilibrium, i.e., the same value of $|B(t)|$ at each time t on all the plateaus between the sheets.

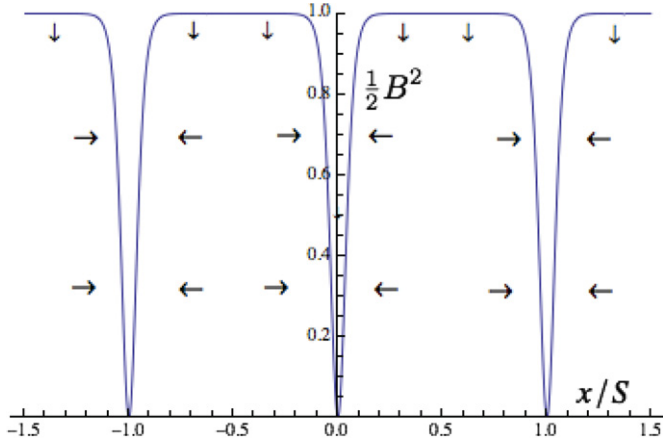


Figure 5. Schematic diagram showing the normalized magnetic pressure distribution $(1/2)B^2$ during the diffusive phase; the inflow into the current sheets is indicated by the horizontal arrows. The downward-pointing arrows indicate the resulting slow decrease of $(1/2)B^2$ as implied by Equation (50).

(A color version of this figure is available in the online journal.)

the dimensionless form of Equation (47), as required for consistency.

We may now seek a similarity solution of Equation (51) of the form

$$B(x, t) = \bar{B}(t)f(\xi), \quad u(x, t) = u_0(t)g(\xi), \quad \text{with } \xi = x/\sigma(t). \quad (55)$$

The time-dependent factor on both sides of Equation (51b) is the same provided that $\sigma(t)\bar{B}(t)$ is constant, i.e., $\sigma(t)$ grows linearly in time; taking

$$\sigma(t) = 2(t + t_1)/S, \quad (56)$$

Equations (51) reduce to

$$f' = fg + C, \quad g' = f^2 - 1, \quad (57)$$

just as for the steady state, but now $\bar{B}(t)$ decreases according to Equation (50), and the layer thickness $\sigma(t)$ increases according to Equation (56). A solution with $f(0) = g(0) = 0$, $f(\infty) = 1$ exists only if $C = 1$, and then the solution is

$$f(\xi) = -g(\xi) = \tanh \xi, \quad (58)$$

much as for the steady current sheet. Thus, in the transition from the initial relaxation phase to the diffusive phase, the field profile within the sheet must evolve from the solid to the dashed curve in Figure 2.

The quasi-static evolution of this diffusive stage continues until the current sheets centered on $x = 0$ and $x = S$ begin to overlap. This occurs when $\sigma(t) \sim S/2$, i.e. (restoring the time dimension, and recalling that $t_1 = O(S)$), when

$$t \sim (S^2/4)t_r, \quad (59)$$

and at this stage, the quasi-static approximation breaks down. Indeed, for $t \gg (S^2/4)t_r$, the convection term in Equation (8) becomes negligible, and purely diffusive decay, described by the diffusion equation

$$\frac{\partial B}{\partial t} = \frac{\partial^2 B}{\partial x^2}, \quad (60)$$

sets in. Ultimately, therefore, in a “final period of decay,” $B(x, t)$ decays exponentially in its fundamental mode in $-S < x < S$, for which $B \sim \sin(\pi x/S) \exp[-(\pi/S)^2 t]$.

It is now apparent that, as anticipated in Section 2, we can distinguish *three* phases in the relaxation/diffusion process:

1. $t/t_r < O(\ln S)$: the fast relaxation phase, with exponentially rapid formation of current sheets near null points of B on the relaxation timescale t_r ;
2. $O(\ln S) < t/t_r < O(S^2/4)$: the slow diffusion phase, during which $|B|$ decreases in inverse proportion to time; the result (50) implies that the timescale $|d \ln \bar{B}/dt|^{-1}$ for this algebraic decay increases from $O(S)t_r$ to $O(S^2)t_r$ during this phase;
3. $t/t_r > O(S^2/4)$: the final phase of (linear) exponential decay on a timescale $O[(S/\pi)^2]t_r$.

As regards the decay of energy, taking account of Equation (50), this is given during the diffusive phase by

$$\frac{1}{2} \langle B^2 \rangle = \frac{S^2}{4(t + t_1)^2}. \quad (61)$$

To extend the range to include the final period of decay, we may merely include an exponential decay factor corresponding to the slowest decaying fundamental mode:

$$\frac{1}{2} \langle B^2 \rangle = \frac{S^2}{4(t + t_1)^2} \exp \left[-2 \left(\frac{\pi}{S} \right)^2 t \right]. \quad (62)$$

5. NUMERICAL SOLUTION OF THE RELAXATION EQUATIONS

For the purpose of computation, we consider an initial field $B(x, 0) = B_0(x)$ periodic in x , with period $2L$, and we continue to use $B_0 = \langle |B_0(x)| \rangle$ as the “unit” of magnetic field. With the further scalings x^{**}, t^*, u^{**} as defined in Equations (22) and (41) (so that when $x = L$, $x^{**} = L/\delta_m = S$), Equations (8) and (7) become (dropping the stars)

$$\frac{\partial B}{\partial t} = \frac{\partial^2 B}{\partial x^2} - \frac{\partial}{\partial x}(uB), \quad \frac{\partial u}{\partial x} = \frac{1}{2}[B^2(x, t) - \langle B^2(x, t) \rangle], \quad (63)$$

and the initial and boundary conditions become

$$B(x, 0) = B_0(x), \quad B(0, t) = 0, \quad B(S, t) = 0, \quad (64)$$

where the scaled initial $B_0(x)$ satisfies

$$\langle |B_0(x)| \rangle = 1. \quad (65)$$

We solve Equation (63) numerically for two representative choices of $B_0(x)$ satisfying Equations (64) and (65), using an explicit finite-difference scheme on a uniform grid of 500 points.

5.1. Sinusoidal Initial Field

Figure 6 shows the evolution with $B_0(x) = (\pi/2) \sin(\pi x/S)$ with $S = 50$. As t increases from 0 to 4 (left-hand column), the field relaxes rapidly and current sheets are formed at the null points of the field $x = 0, 50$, and 100. Between these points, plateaus are formed, while the flux is conserved. At around $t = 4$, the field gradient is so large near the null points that diffusion and flux annihilation become significant. The right-hand panels show the subsequent slow diffusive evolution from $t = 4$ to $t = 400$. The field and the velocity gradient remain approximately uniform on the plateaus, the level adjusting to

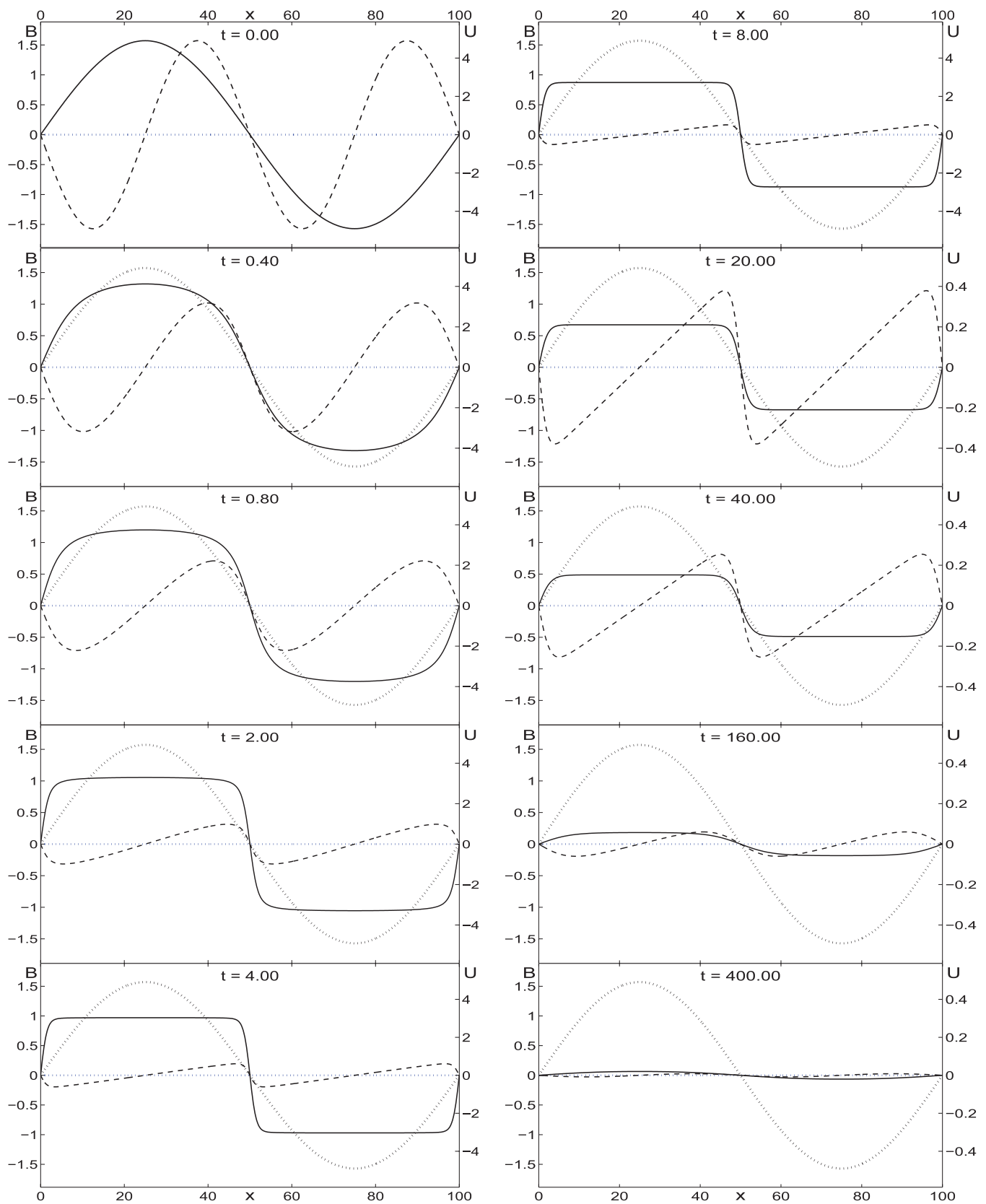


Figure 6. Relaxation of the initial field $B_0(x) = (\pi/2) \sin(\pi x/S)$ with $S = 50$, as governed by Equation (63). Each panel shows the initial field $B_0(x)$ (dotted), the relaxing field $B(x, t)$ (continuous), and the velocity field $u(x, t)$ (dashed). The left column shows the initial nearly non-diffusive relaxation on the short timescale and the formation of current sheets (see Figure 1). The right column shows the subsequent slow diffusive decay. Note the change of velocity scale (shown on the right of the panels) at $t = 20$.

(A color version of this figure is available in the online journal.)

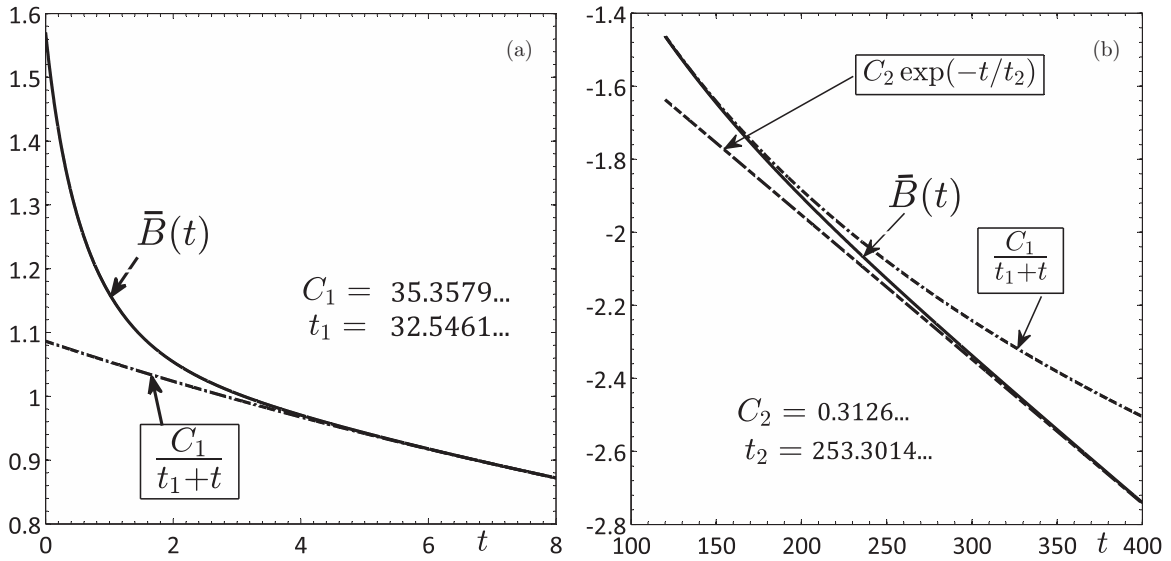


Figure 7. (a) Transition from initial rapid, ideal relaxation to the quasi-static, algebraic decay (liner plot); (b) transition to the final period of exponential decay (semi-log plot).

the annihilation of flux at the null points, as well described by the model of Section 4.2.

The maximum value of the field (at $x = 25$), $\bar{B}(t)$, is plotted in Figure 7 for the initial period ($0 < t < 8$) on the left and for the decay period ($100 < t < 400$) on the right. With $S = 50$, $\ln S \approx 3.91$, and this is indeed roughly the time when diffusion effects become important. Moreover, $S/\sqrt{2} \approx 35.3553$, close to the coefficient $C_1 = 35.3579$ (Figure 7(a)) that provides the optimal fit to the algebraic decay; and the value $t_1 \approx 32 \approx (2/3)S$ is of order S as expected. Finally, $(S/\pi)^2 \approx 253.303$ is close to the value $t_2 = 253.3014$ (Figure 7(b)), the time characteristic of the final period of decay. Thus, the numerical results are entirely consistent with the foregoing theoretical analysis.

5.2. Field with Several Null Points

Figure 8 shows the field evolution for the more structured initial condition:

$$\begin{aligned} B_0(x) &= c \phi(x), \\ \phi(x) &= 10 \sin(2\pi x/S) - 5 \sin(3\pi x/S) + 6 \sin(5\pi x/S) \\ &\quad + 10 \sin(7\pi x/S), \end{aligned} \quad (66)$$

with $S = 50$ and $c = \langle |\phi(x)| \rangle^{-1} = 0.112265$, the prefactor needed to satisfy the normalization condition (65). The field is antisymmetric about the fixed null point $x = S$, i.e., $B(S+x, t) = -B(S-x, t)$. As expected, the field rapidly relaxes to the level ± 1 between the null points, but signs of diffusion are already evident (e.g., near $x = 30$) by time $t = 1$. The slow diffusive stage lasts from about $t = 2$ until $t = 100$, by which time the plateaus have disappeared and the final period of decay has set in. Current sheets at adjacent null points are of opposite sign, and those that are initially close merge and disappear early in the diffusive stage. By time $t = 5$, only three internal null points remain, the one at $x = 50$, and two on either side. These two were initially at approximately $x = 50 \pm 14$, but they move, and during the final period of decay this movement is toward the end points $x = 0$ and $x = 100$, where they are “absorbed.” By time $t = 500$, only the fundamental mode $\sim \sin(\pi x/S)$ remains.

6. EVOLUTION OF THE DENSITY FIELD $\rho(x, t)$

We come now to what is perhaps the most interesting aspect of this problem, namely, the evolution of the density field $\rho(x, t)$, which, as already observed, is closely coupled with that of the magnetic field $B(x, t)$. Consider as before the simple example

$$B(x, 0) = (\pi/2) \sin(\pi x/S) \quad (0 \leq x \leq 2S), \quad (67)$$

with initial density $\rho(x, 0)$ normalized to 1. Let $\Phi_0(X)$ and $M_0(X)$ represent the initial flux and mass contained in the interval $0 < x < X$, i.e.,

$$\begin{aligned} \Phi_0(X) &= \int_0^X B(x, 0) dx = \frac{1}{2} S (1 - \cos \pi X/S), \\ M_0(X) &= \int_0^X \rho(x, 0) dx = X. \end{aligned} \quad (68)$$

Let $X \rightarrow x(X)$ be the net Lagrangian displacement of the fluid particle initially at position X over the entire relaxation process. We know that the relaxed field in $0 < x < S$ is simply $B_r(x) = 1$, so that

$$\Phi_r(x) = \int_0^x B_r(x') dx' = x \quad (0 < x < S). \quad (69)$$

Since flux is conserved during non-diffusive relaxation, $\Phi_r(x) = \Phi_0(X)$, so

$$x/S = \frac{1}{2} [1 - \cos(\pi X/S)] = \sin^2(\pi X/2S). \quad (70)$$

Now let the density distribution in the relaxed state be $\rho_r(x)$, and let

$$M_r(x) = \int_0^x \rho_r(x') dx'. \quad (71)$$

Since mass is also conserved, $M_r(x) = M_0(X)$, so

$$M_r(x) = X = (2S/\pi) \sin^{-1} \sqrt{x/S}. \quad (72)$$

Hence,

$$\rho_r(x) = \frac{dM_r}{dx} = \frac{S}{\pi \sqrt{x(S-x)}} \quad (0 < x < S), \quad (73)$$

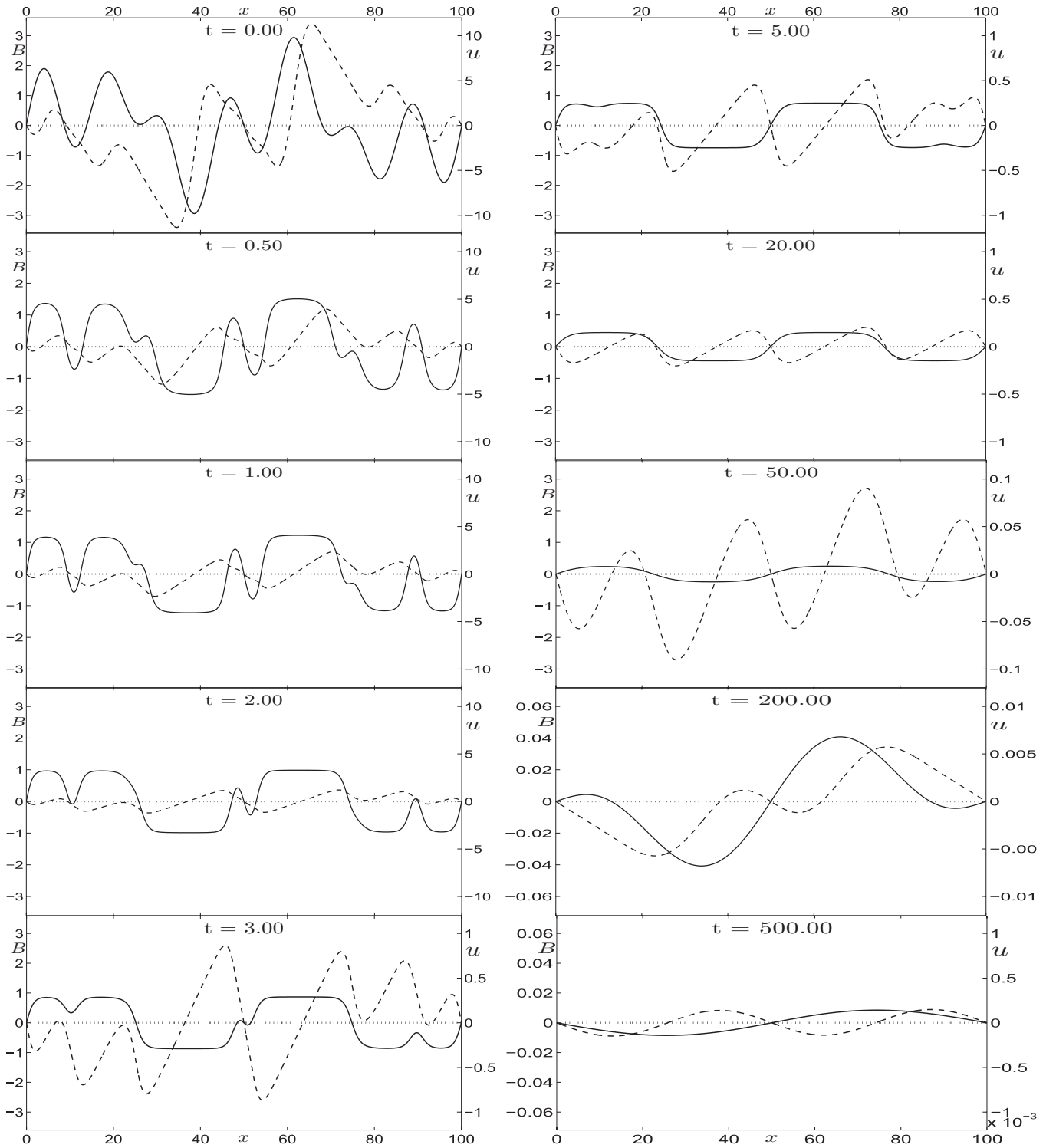


Figure 8. Similar to Figure 6, but with initial condition (with several null points) $B_0(x) = c\phi(x)$, where $\phi(x) = 10\sin(\pi x/S) - 5\sin(3\pi x/2S) + 6\sin(5\pi x/2S) + 10\sin(7\pi x/2S)$, $S = 50$, and $c = \langle |\phi(x)| \rangle^{-1} = 0.112265$. Each panel shows the relaxing field $B(x, t)$ (continuous) and the velocity field $u(x, t)$ (dashed). Until about $t = 2$, relaxation proceeds on the short timescale, although signs of diffusion are already apparent by $t = 1$. Later (right-hand column), the decay is on the slow diffusive timescale. Current sheets at adjacent null points are of opposite sign, and these merge and disappear during diffusive decay. For $t > 250$, only one interior null point remains, and the subsequent decay is similar to that of Figure 6. Note again the changes of scale of u (on the right of the panels) and of B (on the left).

and obviously $\rho_r(x + S) = \rho_r(x)$ for all x . This relaxed density field is shown in Figure 9 for $0 < x < 100$ with $S = 50$. Note that, in the range $0 < x < 25$, $\rho_r(x) = 1$ at $x \approx 5.7$; thus, within this range, fluid is transferred from the region $5.7 < x < 25$ to the region $0 \leq x < 5.7$ during the relaxation process.

The buildup to the singularity $\rho_r(x) \sim x^{-\frac{1}{2}}$ near the null point $x = 0$ appears to be generic, i.e., a similar singularity occurs at every null point at which $B = 0$ and $\partial B/\partial x \neq 0$. However, diffusion presumably causes a cutoff at $x \sim S^{-1}$, where $\rho \sim \sqrt{S}$. We may verify this estimate by considering the time development of $\rho(x, t)$ during this initial phase.

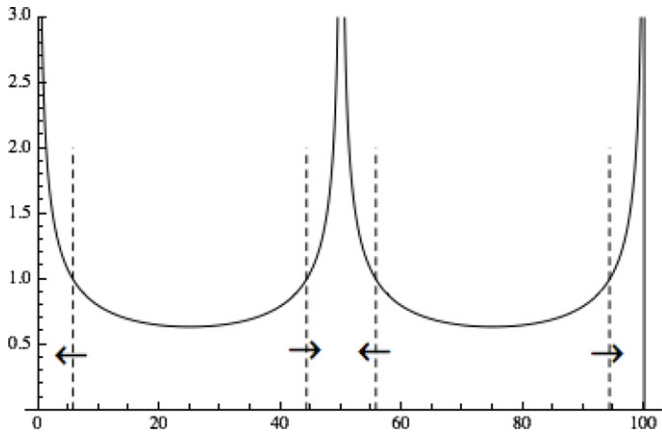


Figure 9. Relaxed density distribution $\rho_r(x)$ in $(0 < x < 2S)$ as given by Equation (73) with $S = 50$ (solid lines). Fluid is transferred during the initial relaxation, as indicated by the arrows, from the central regions toward the current sheets that form at $x = 0, 50,$ and 100 . Dashed lines mark the locations where $\rho_r = 1$, i.e., density has its initial value.

6.1. Initial Buildup of Density near Null Points

As already observed, the density field satisfies

$$\frac{\partial \rho}{\partial t} = -\frac{\partial}{\partial x}(\rho u), \quad (74)$$

and, during the non-diffusive stage, from Equation (38), $\rho u = (1/2)\rho e^{-t}v(\xi)$, with $\xi = xe^t$. Hence,

$$\frac{\partial}{\partial x}(\rho u) = \frac{\partial}{\partial \xi} \left(\frac{1}{2}v(\xi)\rho \right), \quad (75)$$

and Equation (74) becomes

$$2\frac{\partial \rho}{\partial t} + (v + 2\xi)\frac{\partial \rho}{\partial \xi} = -v'(\xi)\rho. \quad (76)$$

With initial condition $\rho(x, 0) = 1$, the symmetry implies that $\rho(-x, t) = \rho(x, t)$ for all $t > 0$.

Now, from Equation (38) and the asymptotic behavior of f , we have

$$v'(\xi) \sim -1 + \xi^2 \quad \text{as } \xi \rightarrow 0, \quad (77)$$

so, near $\xi = 0$, Equation (84) is well approximated by

$$2\frac{\partial}{\partial t}(\ln \rho) + \xi \frac{\partial}{\partial \xi}(\ln \rho) = 1 - \xi^2, \quad (78)$$

or, defining $\zeta = \ln \xi$,

$$2\frac{\partial}{\partial t}(\ln \rho) + \frac{\partial}{\partial \zeta}(\ln \rho) = 1 - e^{2\zeta}. \quad (79)$$

With initial condition $\ln \rho = 0$, the solution to this wave-type equation (as may be verified) is

$$\ln \rho = \frac{1}{2}t - \frac{1}{2}e^{2\zeta}(1 - e^{-t}). \quad (80)$$

Returning to the original variables, this gives

$$\rho(x, t) \sim e^{t/2} \exp[-x^2 e^{2t}(1 - e^{-t})/2], \quad \text{for } |x|e^t \ll 1. \quad (81)$$

Note in particular that

$$\rho(0, t) \sim e^{t/2} \quad \text{and} \quad \partial^2 \rho / \partial x^2|_{x=0} \sim -e^{5t/2} \quad \text{for } t \gg 1. \quad (82)$$

This describes well the buildup of density in a layer of thickness $O(e^{-5t/4})$ near $x = 0$. This initial buildup of density at $x = 0$ continues until $e^{-t} = O(S^{-1})$, by which time

$$\rho(0, t) \sim S^{\frac{1}{2}}, \quad (83)$$

consistent with the previous estimate.

6.2. Concentration of Density at Null Points during Diffusive Phase

We now focus on the continuing and persistent buildup and concentration of density at null points during the diffusive phase, when, as we have seen, there is a continuing inflow into each current sheet from both sides. Consider first a stationary null point at which $u = 0$ (as, for example, the null point at $x = S$ in Figures 6 and 8). From Equations (74) and (51b), we have

$$\frac{\partial \rho}{\partial t} + u \frac{\partial \rho}{\partial x} = -\frac{\partial u}{\partial x} \rho = -\frac{1}{2}(B^2 - \langle B^2 \rangle)\rho, \quad (84)$$

so that, at a stationary null point where $B = u = 0$,

$$\frac{\partial \ln \rho}{\partial t} = \frac{1}{2}\langle B^2 \rangle \approx \frac{S^2}{4(t + 2S/3)^2} \exp\left[-2\left(\frac{\pi}{S}\right)^2 t\right], \quad (85)$$

using Equation (62). Here, we have adopted the (admittedly heuristic) estimate $t_1 = 2S/3$, as found numerically.

This equation can be integrated in terms of the incomplete gamma function. Figure 10(a) shows the buildup of ρ for $S = 50$, up to the time $t \approx 500$ by which the null-point density has saturated at the high value ρ_{\max} somewhat greater than 2×10^5 . Figure 10(b) shows the very sensitive dependence of this saturation level on S : it increases to a value of order 10^6 with the modest increase of S to 55. In fact, for large S , the asymptotic behavior is given by

$$\ln \rho_{\max} \sim \frac{3S}{8} - \frac{\pi^2}{2} \left(1 + \frac{4\pi^2}{3S}\right) \left(-\gamma + \ln\left(\frac{3S}{4\pi^2}\right) + \frac{4\pi^2}{3S}\right), \quad (86)$$

where $\gamma = 0.5772\dots$ is Euler's constant. This result is quite accurate for $S > 30$ and implies approximately exponential growth of ρ_{\max} with increasing S .

In general, however, null points are not stationary: they move with a velocity v that differs from the local fluid velocity u because of diffusion. If, however, $\partial^2 B / \partial x^2$ is small at the null points, then the null point does move with the fluid, and for as long as this is true, Equation (85) holds in the Lagrangian form

$$\frac{D \ln \rho}{Dt} = \frac{S^2}{4(t + 2S/3)^2} \exp\left[-2\left(\frac{\pi}{S}\right)^2 t\right], \quad (87)$$

where D/Dt represents differentiation following the null point. It would appear then that the density will still build up exponentially at the null point, despite its motion, at least until it merges with a neighbor.

This prediction is well supported by numerical computation (see Figure 11). Here again $S = 50$, but this S is based on the half-period of the field (66); the more relevant choice of length scale is here the mean separation \bar{L} of the nulls of B early on in

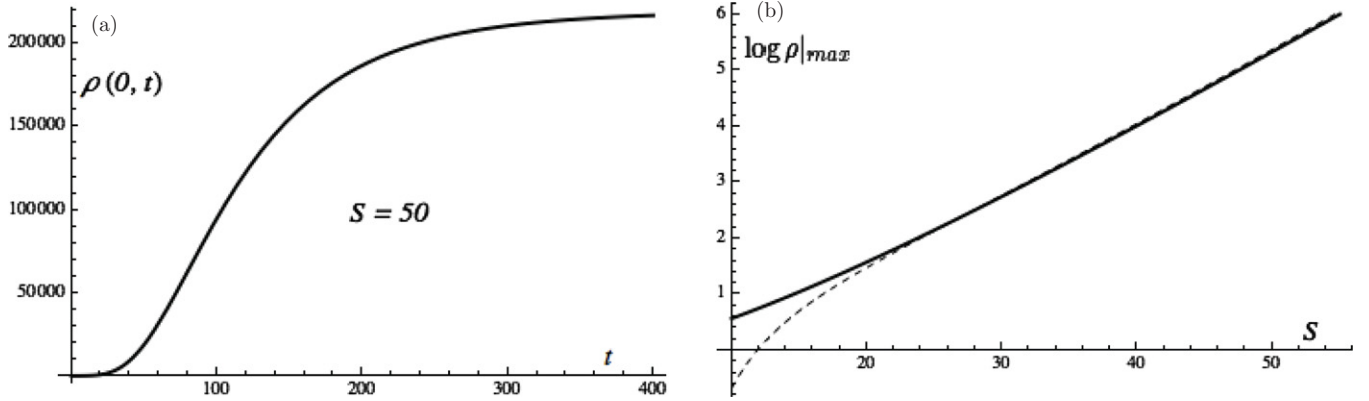


Figure 10. (a) Density buildup at a stationary null point as a function of time for $S = 50$. The saturation level is $\rho_{\max} = 219,817$. (b) $\log_{10} \rho_{\max}$ as a function of S in the range $10 < S < 55$; the asymptotic formula (86) is shown by the dashed curve, which is evidently accurate for $S > 30$.

the diffusive stage (at $t = 5$ say), giving a corresponding $\bar{S} \approx 25$. After the disappearance of a null point, the associated density concentration survives as a fossil and continues to drift with the local fluid velocity. The growth of $\log_{10} \rho$ to between 2 and 2.4 at the principal maxima is compatible with Figure 10(b); in fact, the formula (86) with S replaced by $\bar{S} = 25$ gives $\log_{10} \rho_{\max} \approx 2.14$ (i.e., $\rho_{\max} \approx 138$). (With the modest increase of \bar{S} to 26.5, ρ_{\max} increases to approximately 213.)

Figure 12 shows the density distribution at time $t = 1000$, when no further change is detectable, and also the associated mass concentrations near the spikes of density. The peak density at $x = 50$ is just greater than 200, and 20% of the initial mass is concentrated in the immediate neighborhood ($49.4 < x < 50.6$) of this point. Overall, 84% of the initial mass is concentrated near the five density spikes, and 16% remains in the “evacuated” regions (where $\rho < 1$) between the spikes. The concentration of mass, as well as density, is thus quite striking.

Fluid pressure will also build up at null points in step with density, and this is a possible limiting factor. In this case, it is the sum of magnetic and internal energies that will be minimized during the quasi-steady phase of decay. A further limiting factor is that the exponentially decreasing transverse scale of the density concentrations will eventually be comparable with the mean free path of fluid molecules, and at this stage, if no other mechanism intervenes, the continuum approximation will break down. In cosmic contexts, self-gravitation will of course be a powerful mechanism for the maintenance of localized density concentrations, once formed.

7. POSSIBLE GENERALIZATIONS

The one-dimensional model treated in this paper was chosen for simplicity, and because it permits detailed analysis. We can now, however, envisage generalization to 2D fields.

First, we may consider a field of the form

$$\mathbf{B} = B(x, y, t) \hat{e}_z \quad \text{with} \quad B_0 = \langle |B| \rangle, \quad \langle B \rangle = 0, \quad (88)$$

where the angular brackets now indicate an average over the (x, y) plane; B_0 is conserved in the limit $\eta = 0$. This field is still unidirectional, but a function of position in the plane. The contours $B = \text{const.}$ determine the topology of the field, and this topology is also conserved in this limit. The particular contours $B = 0$ may be described as “null contours,” and these now play a key role in the relaxation process. Some of these null contours may be closed, while others may extend without limit. An example is shown in Figure 13.

If the fluid pressure is negligible, then there is again an immediate tendency to smooth out variations of magnetic pressure $(1/2)B^2$. In particular, fluid will be driven toward the null contours. Current sheets and concentrations of density will develop on these contours, and the area inside closed contours will adjust so that magnetic pressure is equalized across every contour in the relaxed state. In such a state, any further area-preserving deformation in the plane will not change the (uniform) magnetic energy and is therefore “dynamically neutral.” Slow magnetic diffusion in each current sheet will again lead to quasi-static algebraic decay of the field. The decay of the current sheets will lead to slow change of the area inside closed null contours, in such a way as to maintain pressure equilibrium. Again, the density field will grow dramatically on these contours and will survive as a fossil after ultimate decay of the magnetic field.

We note that the resulting highly differentiated density field is qualitatively similar to those found by Davis et al. (2012) in their “symmetron model” for structure formation in the early universe, and by Hennebelle et al. (2008) and Banerjee et al. (2009) in their MHD simulations of molecular cloud formation.

We may also consider fields of the form

$$\mathbf{B} = B_2(x, t) \hat{e}_y + B_3(x, t) \hat{e}_z, \quad (89)$$

i.e., two-component fields with rectilinear field lines whose magnitude and direction may change with increase of the coordinate x . What is interesting here is that even if \mathbf{B}^2 is uniform at time $t = 0$, diffusion will in general produce spatial variation of \mathbf{B}^2 for $t > 0$, and this will immediately trigger the dynamic tendency to restore magnetic pressure equilibrium. For example, we might consider a situation in which the \mathbf{B} lines rotate through an angle π , as x increases through a neighborhood of $x = 0$. The two components of \mathbf{B} initially diffuse independently and differently, and a dip of magnetic pressure must develop near $x = 0$. This will presumably lead to field annihilation near $x = 0$, inflow into this region, and a buildup of fluid density similar to that described in Section 6.2.

We may also envisage generalization to 3D fields, but now hoop stress plays a part in conjunction with magnetic pressure. The field will presumably relax to a force-free magnetostatic equilibrium, i.e., a Beltrami field for which $\nabla \times \mathbf{B} = \alpha(\mathbf{x})\mathbf{B}$, for some scalar $\alpha(\mathbf{x})$, as envisaged by Moffatt (1987). To understand the possible structures of such fields remains an extremely challenging problem. We note that Enciso & Peralta-Salas (2012, 2013) have recently made an encouraging start, through proving the existence of a Beltrami field containing

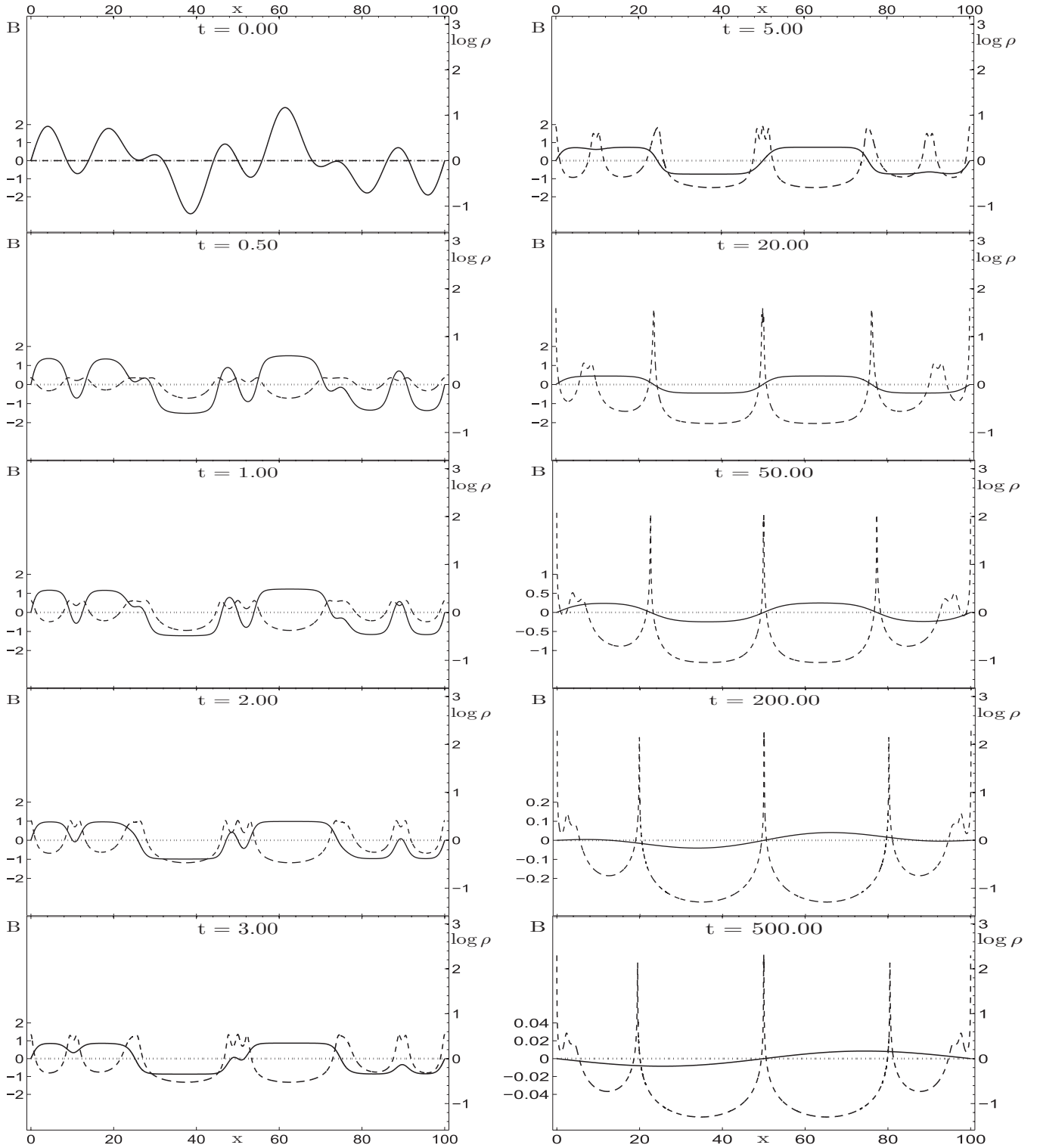


Figure 11. Evolution of density for the same conditions as in Figure 8; the plot shows B (solid, as in Figure 8) and $\log_{10} \rho$ (dashed). Note the changes of scale of B at $t = 50, 200,$ and 500 . The nulls at $x = 0, 50,$ and 100 are stationary, so the density evolves according to Equation (85). The nulls initially near $x = 25, 75$ closely follow material elements (advection dominates diffusion), and, for $t < 100$, the density growth at these moving nulls is almost the same as at stationary nulls. For $t > 100$, the motion of these nulls is dominated by diffusion, so they no longer coincide with local density maxima, which continue to be advected without further growth. The last panel ($t = 500$) shows the ultimate density distribution. Note the remnants of the small local density maxima caused by the pairs of nulls present in the initial condition near $x = 8, 12$ and $x = 88, 92$; these nulls disappear at $t \approx 2$ due to diffusion, and the density maxima later migrate toward the ends of the interval.

any prescribed knot or link among its field lines. 3D fields may also have a chaotic character (as exemplified by the quadratic field of Bajer & Moffatt 1990). As shown by Bajer (2005), the relaxed form of such fields may have stacked current sheets

of non-differentiable structure. Fast reconnection of field lines can occur on an Alfvén timescale (Priest & Forbes 2007); in their treatment of fast reconnection in astrophysical plasmas, Hanasz & Lesch (2003) have concluded that this will occur

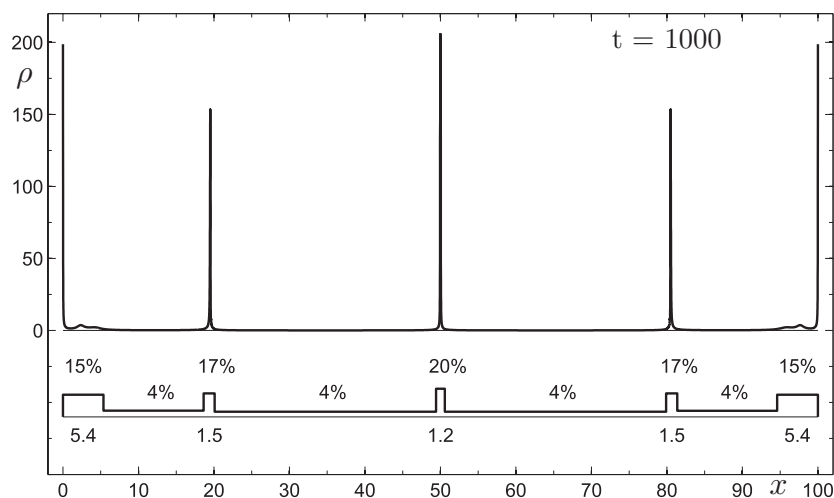


Figure 12. Final distribution of mass at the end of the evolution shown in Figure 11. Upper curve shows density distribution. Lower (step) diagram shows narrow intervals where mass accumulates ($\rho > 1$; i.e., density exceeds its initial value) and broad intervals, which are evacuated ($\rho < 1$). The upper figures (15%, 4%, 17%, ...) give the percentages of the total initial mass left in each interval, while the lower figures (5.4, 1.5, ...) give the widths of the mass concentrations.

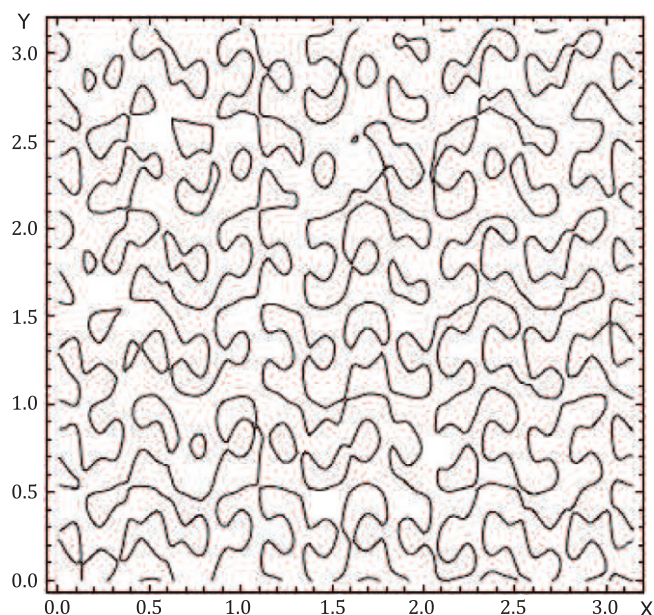


Figure 13. Null contours $B = 0$ for a hypothetical quasi-random 2D field $B(x, y)$, containing 18 Fourier components.

(A color version of this figure is available in the online journal.)

if the plasma β is “significantly larger than $2m_e/m_p$ (twice the ratio of electron mass to proton mass),” i.e., approximately 10^{-3} . For $\beta \ll 10^{-3}$, reconnection can still proceed through the agency of magnetic diffusion as considered in the present paper, this mechanism being most effective, as we have described, near minima of magnetic pressure.

Generalizations of this kind to 2D and 3D fields deserve detailed study and will be the subject of continuing investigation.

We thank the Isaac Newton Institute for Mathematical Sciences (Cambridge, UK) for hospitality during the

program Topological Dynamics in Physical and Biological Sciences, 2012 July–December, and the International Centre for Mathematical Sciences (Edinburgh) for hosting the workshop on Tangled Magnetic Fields in Astro- and Plasma Physics.

One of us (K.B.) is grateful to Trinity College (Cambridge, UK) for the Visiting Fellowship he enjoyed while this work was completed. We acknowledge financial support from EPSRC under grant number EP/I 036060/1.

REFERENCES

- Arnold, V. I. 1974, in Proc. Summer School in Diff. Eqs. at Dilizhan, Erevan, Armenia [In Russian], Armenian Academy of Sciences, Erevan, 229, English translation: 1986 Sel. Math. Sov. 5, 327
- Bajer, K. 2005, *FIDyR*, **36**, 301
- Bajer, K., & Moffatt, H. K. 1990, *JFM*, **212**, 337
- Banerjee, R., & Jedamzik, K. 2004, *PhRvD*, **70**, 123003
- Banerjee, R., Vázquez-Semadeni, E., Hennebelle, P., & Klessen, R. S. 2009, *MNRAS*, **398**, 1082
- Davis, A.-C., Li, B., Mota, D. F., & Winther, H. A. 2012, *ApJ*, **748**, 61
- Doumler, T., & Knebe, A. 2010, *MNRAS*, **403**, 453
- Enciso, A., & Peralta-Salas, D. 2012, *AnMat*, **175**, 345
- Enciso, A., & Peralta-Salas, D. 2013, in IUTAM Procedia, Vol. 7, Topological Fluid Dynamics: Theory and Applications, ed. H. K. Moffatt, K. Bajer, & Y. Kimura (Amsterdam: Elsevier), 13
- Goldstein, R. E., Moffatt, H. K., & Pesci, A. I. 2012, *Nonli*, **25**, R85
- Goldstein, R. E., Moffatt, H. K., Pesci, A. I., & Ricca, R. L. 2010, *PNAS*, **107**, 21979
- Grasso, D., & Rubinstein, H. R. 2001, *PhR*, **348**, 163
- Hanasz, M., & Lesch, H. 2003, *A&A*, **404**, 389
- Hennebelle, P., Banerjee, R., Vázquez-Semadeni, E., Klessen, R. S., & Audit, E. 2008, *A&A*, **486**, L43
- Kulsrud, R. M., & Zweibel, E. G. 2008, *RPPH*, **71**, 046901
- Linardatos, D. 1993, *JFM*, **246**, 569
- Moffatt, H. K. 1985, *JFM*, **159**, 359
- Moffatt, H. K. 1987, *Revista Brasileira de Ciências Mecânicas*, **IX**, 2, 93
- Parker, E. N. 1994, *Spontaneous Current Sheets in Magnetic Fields* (Oxford: Oxford Univ. Press)
- Pfrommer, C., & Dursi, J. 2010, *NatPh*, **6**, 520
- Priest, E., & Forbes, T. 2007, in *Magnetic Reconnection: MHD Theory and Applications* (Cambridge: Cambridge Univ. Press), 616
- Sethi, S. K., & Subramanian, K. 2005, *MNRAS*, **356**, 778
- Tashiro, H., & Sugiyama, N. 2006, *MNRAS*, **368**, 965